CORNELL CBN 96-19
15 November 1996

On Nonlinear Field Components of CESR Elements *

Alexander Temnykh[†]

Laboratory of Nuclear Studies, Cornell University, Ithaca, NY 14853, USA

Introduction

The storage ring operation experience has shown that nonlinear components of leading magnetic field cause many non desired effects. Among them are dynamic aperture limitation, the appearance of the dangerous resonances on betatron tune plane, the beam performance degradation with orbit offset and other. Many of these may be predicted and studied with tracking simulation, if the modeling elements used for tracking contain nonlinearities adequate real. Therefore, the knowledge of the nonlinear field components of storage ring elements may provide the better understanding of storage ring problems and lead to ring improvement.

This paper documents available to date information about nonlinear field components in order to facilitate preparation of the tracking simulation. Data presented here were obtained with magnetic measurenets as well as with POISSON code calculation. Some of data, were published previously, (see [3],[2]). Note that the presented paper does not contain the describtion of the all CESR's elements, but it may happen that it contain data about elements critical for beam dynamic.

The technique used for magnetic field measurement was similar to described in [1]. It was the flipping consisted of few turns, (usually from 1 to 10), made with 100mkm

---

[*] Work supported by the National Science Foundation

[†] On leave from BINP, Novosibirsk

diameter copper wire. Coil was streached throgh magnets, so the signal was proportional to the field integrated over all magnet length. In the most of cases the magnetic field was measured in horizontal plane. So, its vertical components give the normal field distribution and its horizontal components corresponded to skew field.

The following definitions will be used below.

1) The numbering index will show the power of variable corresponding to coefficients. Index $_y$ will indicate vertical magnetic field, i.e., normal components, index $_x$ will be attached to horizontal components.

2) To characterize the quality of magnetic field the variable $\delta B/B$ will be applied. Were B is ideal field and δB is the difference between ideal and measured field.

The following CESR elements are described below:

1) Normal bending magnets (model 201),

2) Horizontal separators,

3) Sextupoles and vertical steerings,

4) Panofsky magnets,

5) IR quads: REC, Q1 and Q2,

6) Q48W quad,

7) Mark II quadrupole magnets,

8) Wigglers

For the first two elements, bending magnet and horizontal separator, data was obtained by calculation, for other elements here are results of magnetic measurements.

In order to reduce the amount of uncertain information the selection of measured data was done. Section about the IR quads presents data for only normal, but no for skew components. It is done because of the measurement has shown that the appearance of skew components is caused by the small asymmetry in the position of quad coils. Its position is unknown for final IR quads assembly in the tunnel. So, the measured skew component may not be adequate real. In addition, the vertical steerings produce much stronger skew components then IR quads. Therefore, it seems reasonable to skip the description of nonlinear skew components in IR quads.

1 Calculation for normal bending magnets, (model 201)

The performance of the normal field bending magnet was calculated with POISSON code using profile given in CESR design report, see figure 4-1 in [6]. The result is shown on figure 1. Here is the variation of the normal field component versus horizontal position. Note that the inner size of vacuum chamber in the bending magnets is about $\pm 4.5\,cm$, and the relative field variation, $\delta B/B$, in here less than $3 \cdot 10^{-4}$. The contribution of the various multipols into field nonuniformity is on the table in figure 1. These numbers may be easy evaluated into field components to use in structure for tracking program.

2 Horizontal separators field quality

The calculated variation of the electrical field generated by horizontal separators is on figure 2. The table shows coefficients which may be used to obtain nonlinear field components. All dimensions of electrostatic plates and another information needed for calculation was given by J. Welch.

3 Sextupoles and vertical steerings

CESR sextupole magnets provide two functions. They are used to generate sextupole field as well as to create horizontal magnetic field for vertical beam steering, see [6]. The both, sextupole and horizontal magnetic fields were measured with long rotating coil of 78 mm diameter. Harmonic analysis gave its multipole content which is in the table 1. Note that measurement was done with coil integrated magnetic field over all magnet length, i.e., it included fringe field. That may cause the difference between data shown in the table and data obtained with Hall probe in [4]. Two columns in the table 1 called *Original tips* and *Modified tips* show data for two different pole tips described in [4].

4 Panofsky magnets

The Panofsky stile magnets located around IP provide vertical/horizontal beam steering as well as a skew quadruple fields for coupling correction. Their coils have two types of windings. The inner one made with #12 copper wire is designed for 30 Amps of maximum current. The second winding done with soft copper 3/16 inch diameter tubing has cooling water flow and may hold 150 Amps of current. The first winding provides beam steering functions while the second one with higher current capability is for skew quad field generation.

There are three types of magnets. The *Type I* magnets are located near by Q5,6,7. They fit regular CESR's vacuum chamber and have smallest aperture. Results of magnetic measurements averaged over 6 samples of these are on table 2 in the column *Type I* . The second type magnets are placed near by Q2. They have bigger aperture and more uniform current distribution along plates then *Type I.* The measured field components for this type are in column *Type II* . The magnets of the third type are placed next to Q1. They have the same as *Type II* dimensions but different number of turns into inner winding. Their field components are presented in column *Type III* .

5 IR quads: REC, Q1 and Q2

All IR quads were modified and their magnetic properties were accurately measured during shut down time devoted to crossing angle optic preparation in the summer of 1995. Below are results of these measurements.

Figure 3 gives normal magnetic field variation versus horizontal position for REC quads. Table under the plot shows fitting coefficients which may be used to calculate normal nonlinear field components. The skew components for the both East and West REC quads were less then $5 \cdot 10^{-4}$ of the normal magnetic field.

Figures 4 and 5 show magnetic field quality of Q1 and Q2 quads. Here are plots for normal field variation measured under near operation condition. Nonlinear field components may be calculated using coefficients given in the tables. The horizontal, i.e., skew field component in all cases was less than $5 \cdot 10^{-4}$ of the normal field.

6 Q48W quad

The Q48W quad is one of the IR type quads provided final focus in north CESR IP, see [6]. The previous measurements made in 1978 by Bruce G. Gibbard, (see [5]), shown less then $\pm 5 \cdot 10^{-4}$ field variation inside used aperture. This result was confirmed with recent measurement reported in [3]. Figure 6 copied from [3] shows that the field variation is less then $\pm 5 \cdot 10^{-4}$ in aperture $\pm 7\,cm$. The table on figure 6 presents coefficients which may be used to calculate nonlinear field components.

7 Mark II quadrupole magnets

Mark II quadrupoles provide beam focusing in arcs, see [6]. Figure 7 shows recently measured normal field variation of one of these. Note that this measurement is in good agreement with old ones dated by 1977.

8 Wigglers

Two permanent magnet wigglers are employed to CESR to generate SR. Result of magnetic measurement of West wiggler was reported in [2] and here is represented on figures 8 and 9. Another one, East wiggler, was measured in in May of 1995. Figures 10 and 11 show its normal and skew components.

9 Conclusion

The undesired effects of the nonlinear field components on CESR performance is not always obvious. They may be masked by the other factors. Let's take one example. It is known that at CESR the poor beam life time limits pretzel at the level which is less then one can predicte using designed vacuum chamber size and beam emittance. One can suspect unknown mechanical aperture limit or the big distortion of beta function with large orbit offset due to errors in sextupole distribution. However the dependence of betatron tunes versus pretzel indicates the presence of the normal nonlinear field component of order higher than sextopoles generate. It is very possible that this nonlinearity leads to beam property degradation with pretzel and gives the pretzel limit.

Using the data presented in this paper in the tracking simulation and combining results of simulation with experiments one can identify the sours of nonlinearity and then fix it. However, it may occur that the bad elements is not among described above. In this case more investigation must be done.

References

[1] *Developpement de Banc de measure magnetiques pour undulateurs et wigglers*, D.Frachon Thesis, April 1992, ESRF.

[2] *Magnetic Measurement of the West Wiggler in CESR* D. Frachon, I. Vasserman, J. Welch and A. Temnykh, CBN 93-7

[3] *Q48W magnetic measurement*, A. Temnykh, CON 96-06

[4] *CESR sextupole upgrade*, A. Michailichenko, CON 96-05

[5] *Interaction Region Quadrupole Report* Bruce G. Gibbard, CBN 78-12

[6] *A Desigh Report for the CORNELL ELLECTRON STORAGE RING*, Cornell University, Laboratory of Nuclear Studies, April 1977

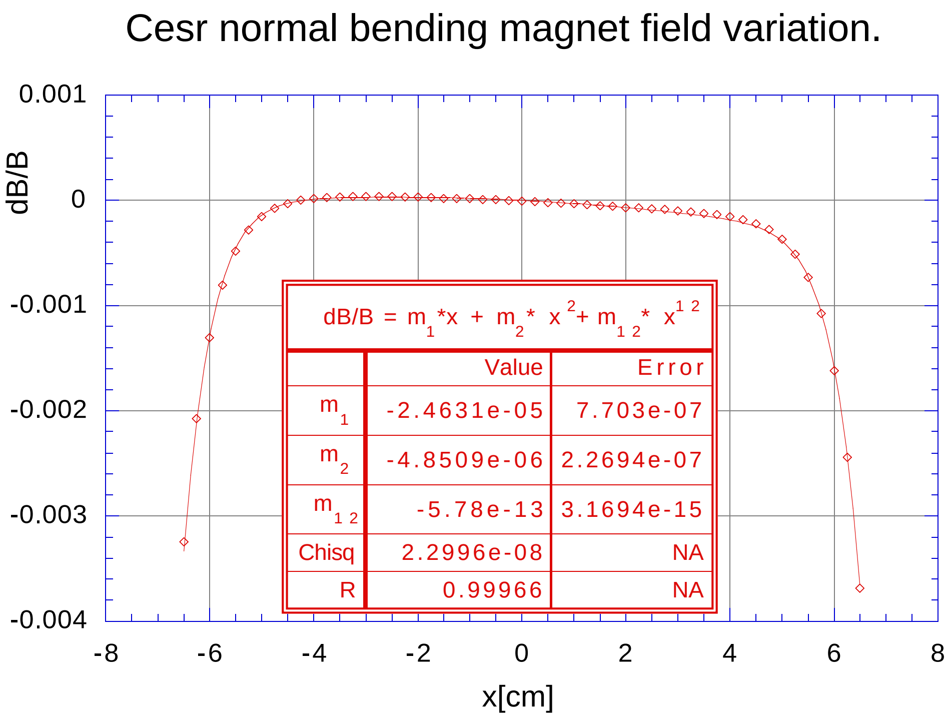

Cesr normal bending magnet field variation.

$dB/B = m_1 * x + m_2 * x^2 + m_{12} * x^{12}$

	Value	Error
m_1	-2.4631e-05	7.703e-07
m_2	-4.8509e-06	2.2694e-07
m_{12}	-5.78e-13	3.1694e-15
Chisq	2.2996e-08	NA
R	0.99966	NA

Figure 1: Calculated bending magnet field variation in the mid-plane (y=0), model 201.

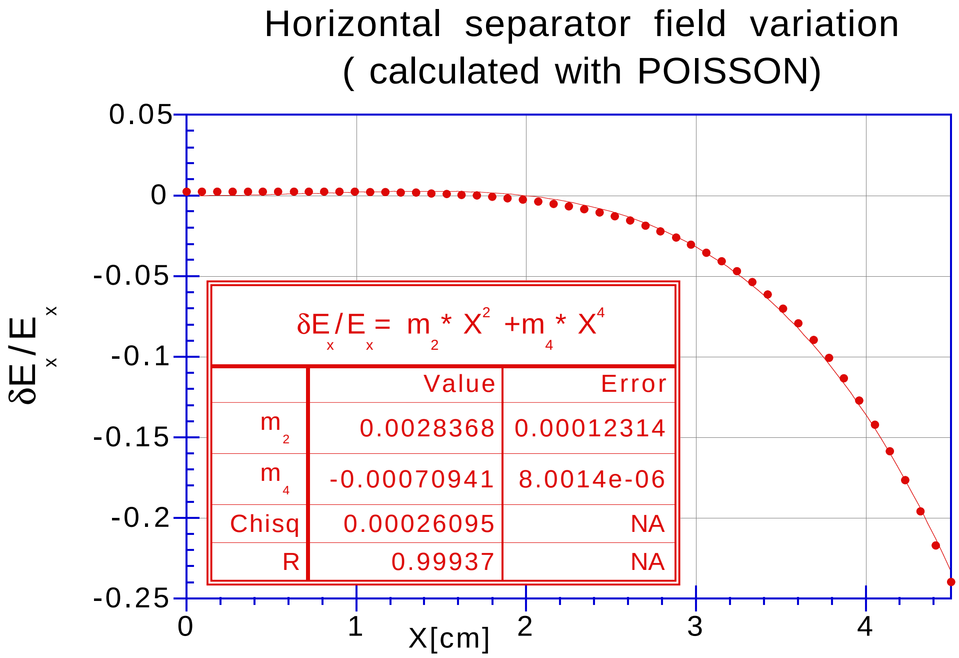

Figure 2: Calculated horizontal separator field variation in a mid-plane (y=0).

Component	Units	*Original tips*	*Modified tips*
Sextupole function			
$B_{y,2}$	$\frac{gauss \cdot m}{cm^2 Amp}$	1.51	1.062
$B_{y,8}$	$\frac{gauss \cdot m}{cm^8 Amp}$	$-2.1 \cdot 10^{-5}$	$3.8 \cdot 10^{-6}$
Vertical steering function			
$B_{x,0}$	$\frac{gauss \cdot m}{Amp}$	22.45	19.82
$B_{x,4}$	$\frac{gauss \cdot m}{cm^4 Amp}$	-0.028	-0.015

Table 1: Magnetic field components of sextupole magnets.

Figure 3: The field variation of West and East REC quads measured in the mid-plane (y=0).

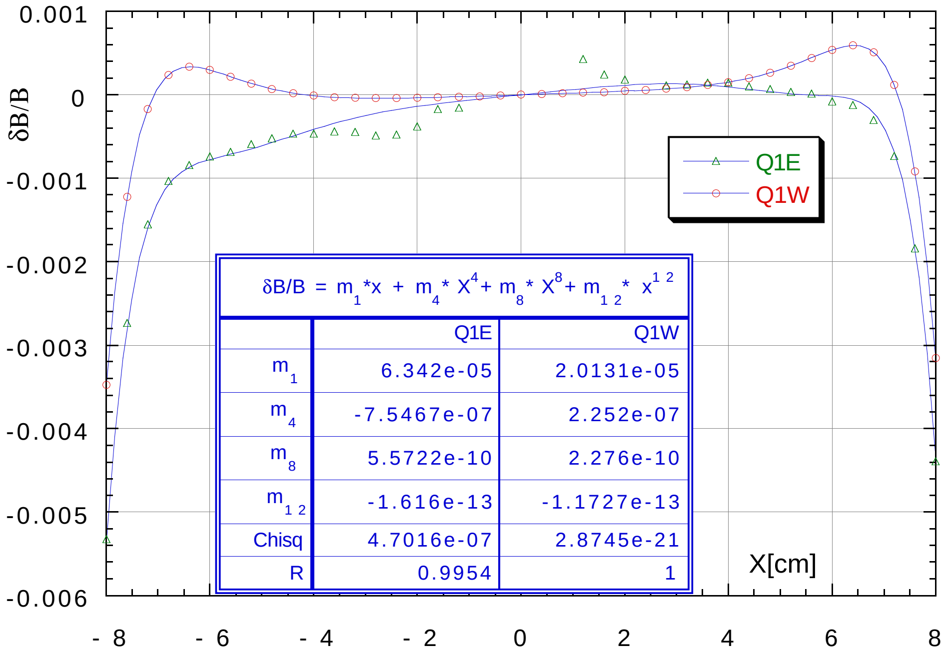

$\delta B/B = m_1 * x + m_4 * X^4 + m_8 * X^8 + m_{12} * x^{12}$

	Q1E	Q1W
m_1	6.342e-05	2.0131e-05
m_4	-7.5467e-07	2.252e-07
m_8	5.5722e-10	2.276e-10
m_{12}	-1.616e-13	-1.1727e-13
Chisq	4.7016e-07	2.8745e-21
R	0.9954	1

Figure 4: The field variation of Q1E and Q1W quads (95 cm long, 140 mm pole diameter) measured in the mid-plane (y=0).

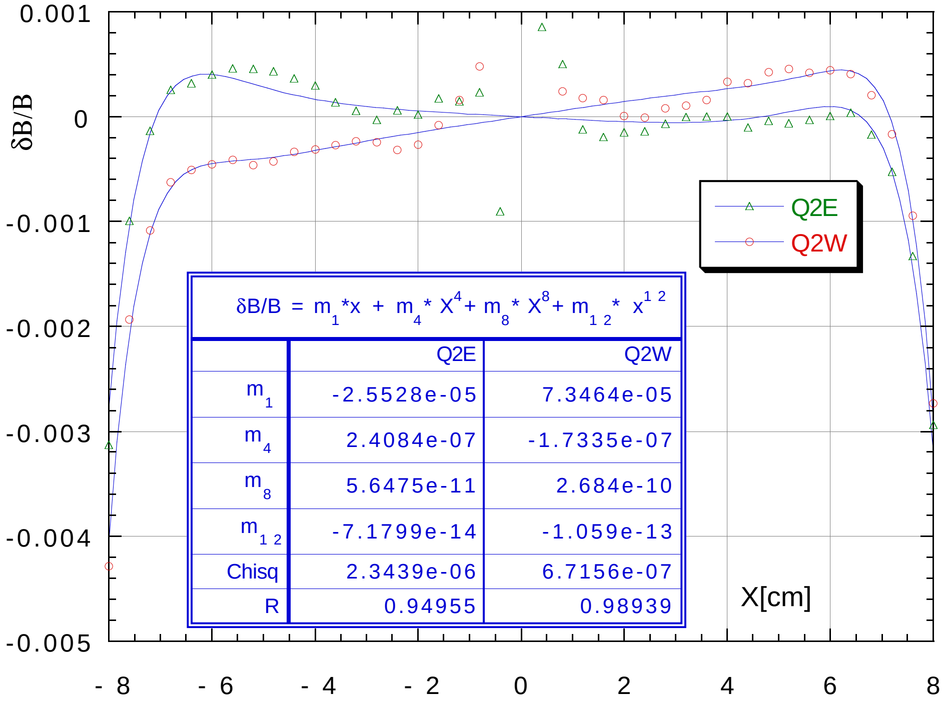

$\delta B/B = m_1 {*} x + m_4 {*} X^4 + m_8 {*} X^8 + m_{12} {*} x^{12}$

	Q2E	Q2W
m_1	-2.5528e-05	7.3464e-05
m_4	2.4084e-07	-1.7335e-07
m_8	5.6475e-11	2.684e-10
m_{12}	-7.1799e-14	-1.059e-13
Chisq	2.3439e-06	6.7156e-07
R	0.94955	0.98939

Figure 5: The field variation of Q2E and Q2W quads (65 *cm* long, 150 *mm* pole diameter) measured in the mid-plane (y=0).

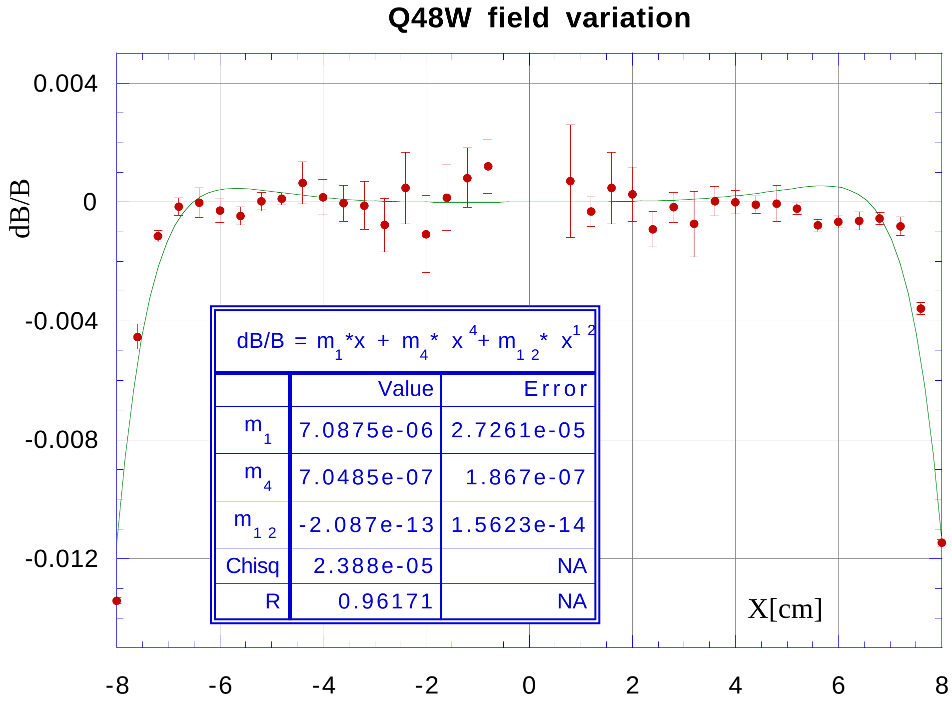

$dB/B = m_1 * x + m_4 * x^4 + m_{12} * x^{12}$

	Value	Error
m_1	7.0875e-06	2.7261e-05
m_4	7.0485e-07	1.867e-07
m_{12}	-2.087e-13	1.5623e-14
Chisq	2.388e-05	NA
R	0.96171	NA

Figure 6: The field variation of Q48West quad (65 cm long, 120 mm pole diameter) measured in the mid-plane (y=0).

Figure 7: The field variation of Mark II quad measured in the mid-plane (y=0).

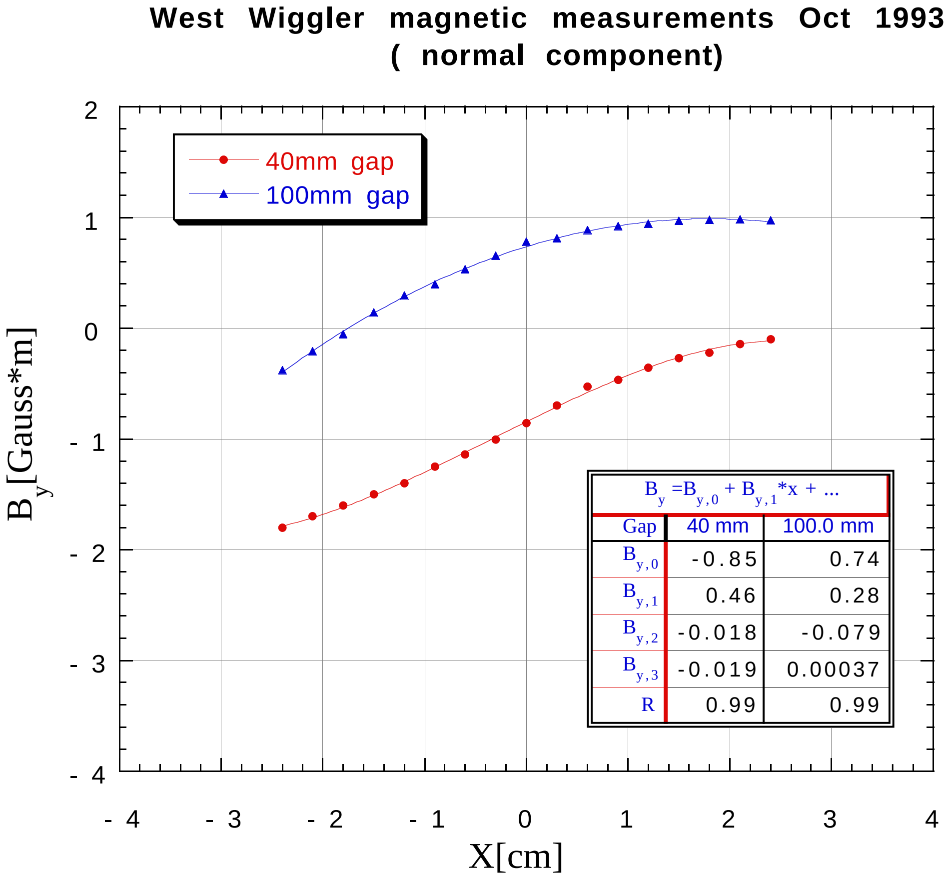

$B_y = B_{y,0} + B_{y,1}*x + \ldots$

Gap	40 mm	100.0 mm
$B_{y,0}$	-0.85	0.74
$B_{y,1}$	0.46	0.28
$B_{y,2}$	-0.018	-0.079
$B_{y,3}$	-0.019	0.00037
R	0.99	0.99

Figure 8: Normal component of West Wiggler field integrated over wiggler's length

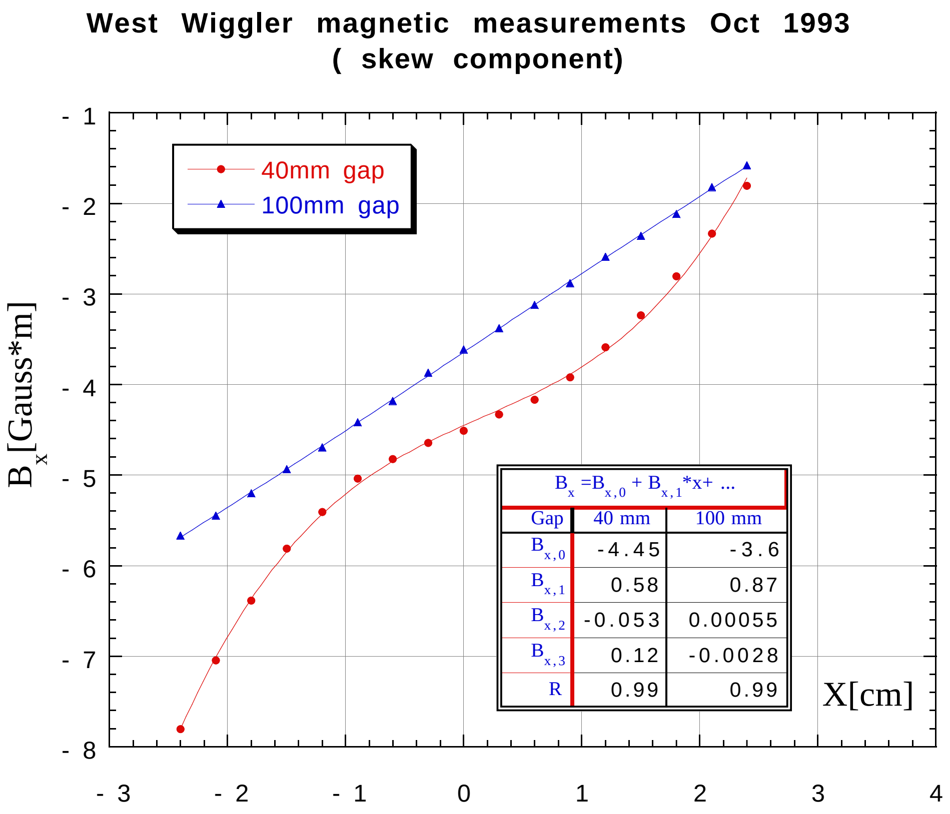

$B_x = B_{x,0} + B_{x,1} * x + \ldots$		
Gap	40 mm	100 mm
$B_{x,0}$	-4.45	-3.6
$B_{x,1}$	0.58	0.87
$B_{x,2}$	-0.053	0.00055
$B_{x,3}$	0.12	-0.0028
R	0.99	0.99

Figure 9: Skew component of West Wiggler field integrated over wiggler's length

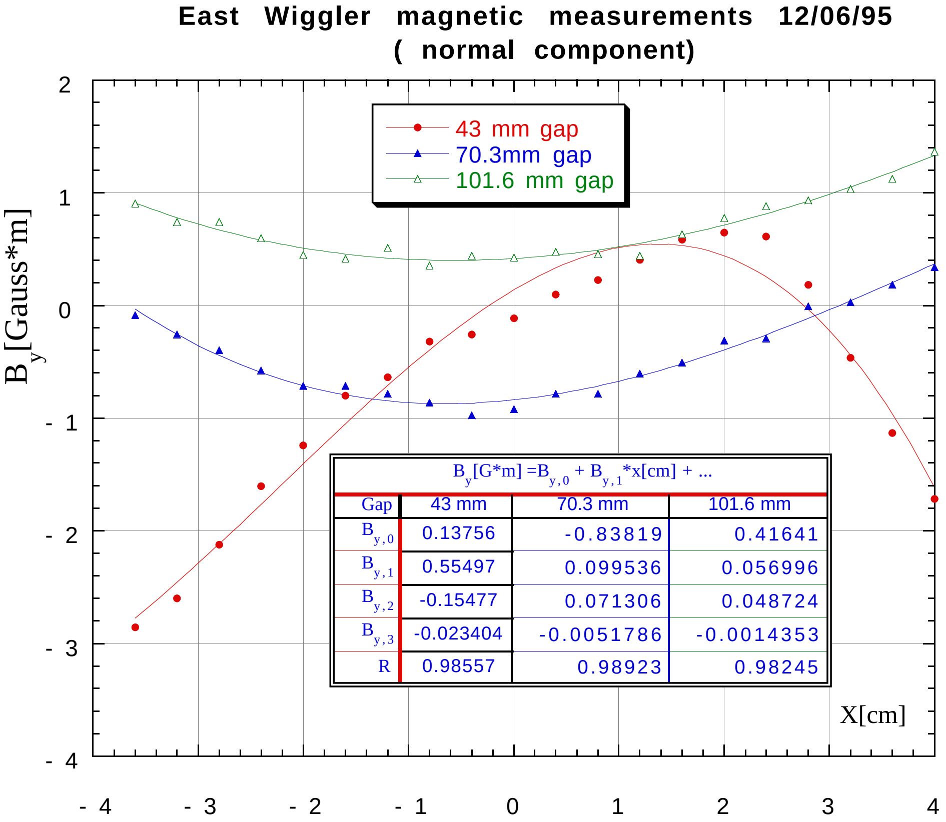

$B_y[G*m] = B_{y,0} + B_{y,1}*x[cm] + \ldots$

Gap	43 mm	70.3 mm	101.6 mm
$B_{y,0}$	0.13756	-0.83819	0.41641
$B_{y,1}$	0.55497	0.099536	0.056996
$B_{y,2}$	-0.15477	0.071306	0.048724
$B_{y,3}$	-0.023404	-0.0051786	-0.0014353
R	0.98557	0.98923	0.98245

Figure 10: Normal component of East Wiggler field integrated over wiggler's length

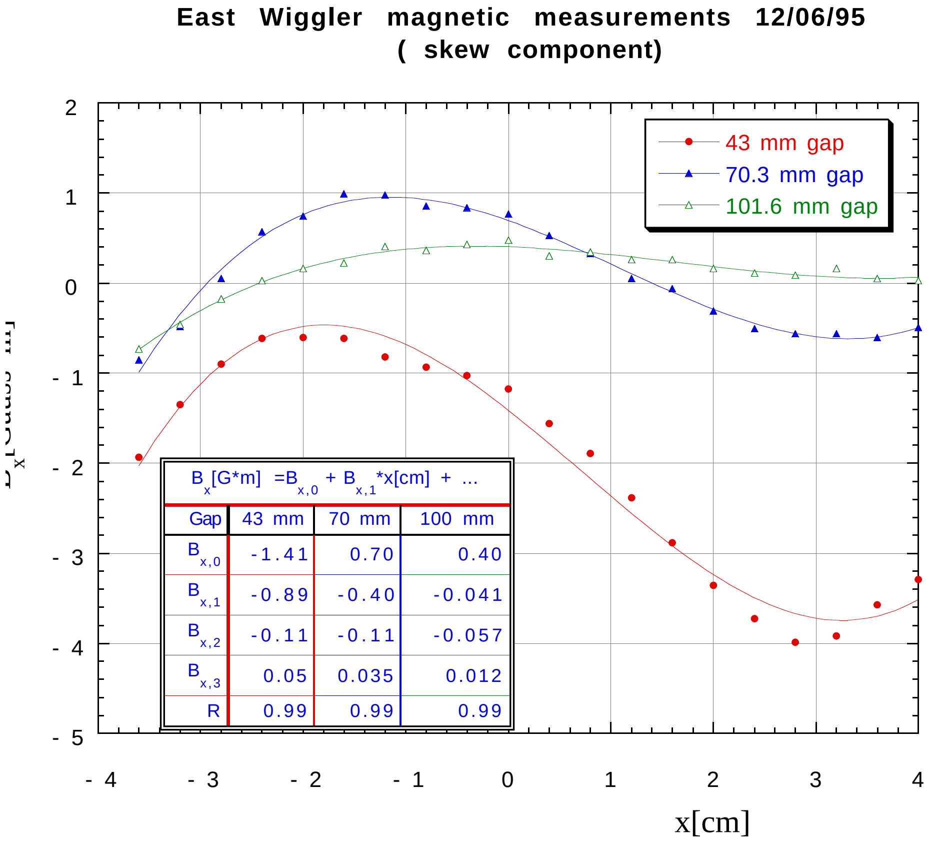

$B_x[G*m] = B_{x,0} + B_{x,1}*x[cm] + \dots$

Gap	43 mm	70 mm	100 mm
$B_{x,0}$	-1.41	0.70	0.40
$B_{x,1}$	-0.89	-0.40	-0.041
$B_{x,2}$	-0.11	-0.11	-0.057
$B_{x,3}$	0.05	0.035	0.012
R	0.99	0.99	0.99

Figure 11: Skew component of East Wiggler field integrated over wiggler's length